

# Study of the Effect of some Deflector's Geometry Factors on the Reduction of the Aerodynamic Drag of the Car Model

Mohamed MAINE<sup>a\*</sup>, Mohamed EL OUMAMI<sup>b</sup>, Otmane BOUKSOUR<sup>b</sup>, Boujemâa NASSIRI<sup>c</sup>

<sup>a</sup>Higher National School of Electricity and Mechanics, University Hassan II of Casablanca, Road of El Jadida, km 7, PB: 8118, Oasis, Casablanca, Morocco.

<sup>b</sup>Laboratory of Production, Mechanics and Industrial Engineering, Higher School of Technology, University Hassan II of Casablanca, km 7, PB: 8118, Oasis, Casablanca, Morocco.

<sup>c</sup>Sustainable Innovation and Applied Research Laboratory, Universtapolis, Bab Al Madina, Tilila, P.B: 8143, Agadir, Morocco.

Received April 15 2021

Accepted June 23 2021

## Abstract

In this article, passive flow control around a generic car model has been investigated numerically. A deflector installed on the rear window of the Ahmed model at 25° was used to study the aerodynamic effect. The study involves the analysis of a set of eight two-level deflector-related factors with the aim of assessing their effects on aerodynamic drag. The assays were determined by establishing a Plackett-Burman screening plan and the results are studied by JMP Pro 14 software. It was observed that the factors (type of deflector, inlet velocity and length's ratio) have a significant effect on reducing aerodynamic drag. The optimal test conditions proposed by the Plackett-Burman plan were investigated numerically and the value obtained was slightly higher than the value of the screening design. It was concluded that the model of Ahmed with optimal deflector gives the best drag reduction, compared to the model without deflector. Installing the optimal deflector on Ahmed's body widens the wake area and eliminates chainstay vortex.

© 2021 Jordan Journal of Mechanical and Industrial Engineering. All rights reserved

**Keywords:** Aerodynamic drag, Generic car, Ahmed model, Deflector, Plackett-Burman plan;

## Nomenclature

<i>ANN</i>	Artificial Neural Network
<i>ANOVA</i>	Analysis Of Variance
<i>CFD</i>	Computational Fluid Dynamic
<i>CPU</i>	Central Processing Unit
<i>EARSM</i>	Explicit Algebraic Reynolds Stress Model
<i>RANS</i>	Reynolds Average Navier-Stokes
<i>RSM</i>	Response Surface Method
<i>SST</i>	Shear stress transport
<i>L</i>	Ahmed body length
<i>W</i>	Ahmed body width
<i>l<sub>D</sub></i>	Deflector's length
<i>w<sub>D</sub></i>	Deflector's width
<i>Th</i>	Deflector's thickness
<i>θ</i>	Deflector's angle of inclination
<i>α</i>	Ends angle of the deflector
<i>C<sub>D</sub></i>	Drag coefficient
<i>C<sub>L</sub></i>	Lift coefficient
<i>U<sub>0</sub></i>	Inlet velocity
<i>S<sub>x</sub></i>	Projected area in x direction
<i>ρ</i>	Specific density of the air
<i>k</i>	Turbulent kinetic energy
<i>ω</i>	Specific dissipation rate
<i>ε</i>	Dissipation rate
<i>μ<sub>t</sub></i>	Turbulent viscosity
<i>R<sup>2</sup></i>	Coefficient of determination

## 1. Introduction

The current energy and environmental context requires the search for effective strategies to reduce the energy consumption of ground vehicles. Researchers in the automotive industry have developed methods of modifying the flow around a car [1]. These techniques are mainly divided into two categories, namely: active control and passive control [2]. The first method is to change the shape of the vortices in the wake area, adding additional energy using an instrument installed in a specific location on the vehicle body. Among the active control methods we can cite: synthetic jets [3]; micro-jets with regular blowing [4]; aspiration [5]; fluidic oscillators [6]; Plasma actuator [7] and winglet devices [7, 8].

The passive flow control method involves modifying the flow around the vehicle by adding devices in specific locations. This method uses several techniques: deflectors [10]; rear plates [11]; lateral guide vanes [12]; underbody diffuser [13]; vortex generators [14]; streaks [15]; non-smooth surface [16]; jet boat tail [17]; linking tunnels [18] and rounded edges [19].

There are also several coupled control techniques, namely: Coanda jet effect [20]; ventilation in the slots [21]; blowing and variations of the front geometry [22] and vortex generator network and rear spoiler [23]. Compared to active control, passive control methods do not require sophisticated actuators and electronic control systems,

\* Corresponding author e-mail: mmdmaine@gmail.com.

which ensures greater reliability. In addition, passive control methods have another obvious advantage since they do not require any power supply [24]. In this article, we are interested in using the deflector with optimal parameters as a passive method of reducing aerodynamic drag of cars.

Significant optimization efforts have been made around ground vehicles to minimize the aerodynamic drag. (Krajnovic) [25] used the Response Surface Method (RSM) for aerodynamic optimization of the flow around a train. The overall optimization of the drag coefficient and crosswind stability was obtained by applying the genetic algorithm on the polynomials of the response surface methodology. (Zheng et al.) [26] used artificial neural networks (ANNs) formed by a relatively small number of CFD simulations for aerodynamic optimization. It was found that the ANN approximation reduces the cost of calculations.

(Beigmoradi et al) [27] studied the optimization of the rear of Ahmed model taking into account aerodynamic and acoustic objectives. The Taguchi method with four factors was chosen to reduce the number of simulations. (Wang et al.) [16] performed numerical studies to investigate the reduction in aerodynamic drag of Ahmed model using a fitted non-smooth surface. An aerodynamic optimization method based on a Kriging substitution model was used to design the non-smooth honeycomb surface. Four structure parameters were selected as design variables, and a 16-level experimental design method based on orthogonal tables was used to analyze the sensitivities and influences of the variables on the drag coefficient.

This article looks at the study of the variation of a set of parameters related to the deflector installed on the rear window of Ahmed's model. The Plackett and Burman plan is used to optimize testing in an experiment design method. To our knowledge, this is the first time such an approach has been used to determine the factors that influence aerodynamic drag.

## 2. Studied model

### 2.1. Ahmed model

The complexity of the study of flows around cars requires a simple and standard model to compare the results of different numerical and experimental studies. (Ahmed et al.) proposed a simplified road vehicle model for better analysis and understanding of three-dimensional airflows around the vehicle [28]. Several authors have used Ahmed's model as a reference to study the aerodynamics of road vehicles. It is a generic car geometry comprising a front plate with rounded parts and a sloping rear top surface. The slant angle is adjustable and is the main variable parameter of the model in the experimental research of (Ahmed et al.). Most of the body drag is due to the pressure drag triggered from the rear. The wake structure is very complex with a parting zone and counter-rotating vortices generated at the intersection between the back bank angle and the side edges. The dimensions of the Ahmed model are  $1044 \times 389 \times 288$  mm. The bottom surface of Ahmed's model is 50 mm above

the ground, and four feet are used to support the model. The origin of the coordinates is fixed to the ground at the midpoint of the rear face and the directions of the coordinates are as in Figure 1. In this way, the rear base is tilted  $25^\circ$ .

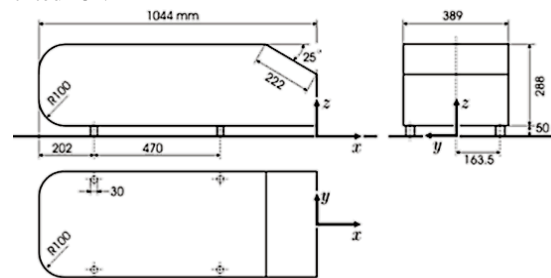


Figure 1. Dimensions of Ahmed model [28].

### 2.2. Deflector

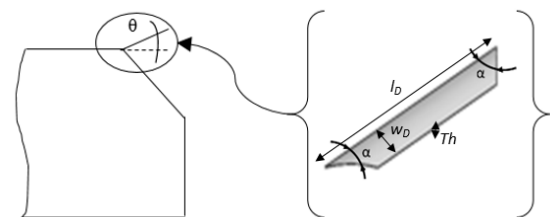


Figure 2. Deflector installed at on the rear slant of Ahmed model

The deflector is a device installed on the rear window of the Ahmed model. It has a length ratio ( $l_D/L$ ), a width ratio ( $w_D/W$ ) and a thickness ( $Th$ );  $l_D$ ,  $w_D$ ,  $L$  and  $W$  are respectively, the length, the width of the deflector, the length and the width of the Ahmed model. The ends of the deflector are cut with an angle  $\alpha$ . The deflector's angle of inclination is  $\theta$  (Figure 2).

In recent years, various works have been carried out around the deflector. (Fourrié et al.) [10] and (Hanfeng et al.) [24] carried out an experimental study on the deflector installed at the rear slant of the Ahmed model for Reynolds numbers between  $7.7 \times 10^5$  and  $8.7 \times 10^5$ . (Raina et al.) [29,30] carried out a numerical study using the RANS model with two different turbulence equations (SST  $k-\omega$  and  $k-\epsilon$ ), for Reynolds numbers between  $7.7 \times 10^5$  and  $9.4 \times 10^5$ . (Fourrié et al.) [10] and (Raina et al.) [29,30] used a 1:1 scale model; while (Hanfeng et al.) [24] have used a 1:2 scale model. The deflector's angle varied from  $0^\circ$  to  $5^\circ$ . The obtained reduction in aerodynamic drag is between 6.6 and 11.8 % compared to their references values cited in Table 1.

The values of the drag coefficient obtained from the two turbulence models are very different. Perhaps this variation is due to the lack of prediction of the near wall sublayer. It has been observed that the drag is influenced by the angle of inclination of the deflector and the Reynolds number. In these studies, the authors used a straight deflector. Their decision variables are mainly the angle of inclination and the flow velocity. They suggest that flow control on such geometries should take into account any flow structures that contribute to wake flow.

**Table 1.** Research work on the Ahmed model with deflector

Author, year	Fourrié, 2011 [10]	Hanfeng, 2016 [24]	Raina, 2017 [29]	Raina, 2018 [30]
Model	Ahmed model with rear slant angle of 25°			
Deflector's angle	5°	0°	5°	5°
Deflector's dimension	389×20×1.2	194.5×10×1.2	389×20×1.2	
Study	Experimental		Numerical	
Turbulence equations	--	--	SST k- $\omega$	k- $\epsilon$
Re	7.7×10 <sup>5</sup>	8.7×10 <sup>5</sup>	7.7×10 <sup>5</sup>	9.4×10 <sup>5</sup>
U <sub>0</sub> (m.s <sup>-1</sup> )	40	25	40	50
C <sub>D</sub>	0.259	0.381	0.318	0.271
Reference *	0.285	0.432	0.340	0.290
% reduction	9 %	11.8 %	7 %	6.6 %

\* C<sub>D</sub> for Ahmed model with rear slant angle of 25° without deflector

**3. Mathematical model**

*3.1. RANS turbulence models*

*3.1.1. Reynolds average*

This average describes the velocity fields statistically. The turbulent flow is divided into two terms (Eqn. 1):

$$u_i = U_i + u'_i \tag{1}$$

Where  $U_i$  is the average value of the freestream velocity and  $u'_i$  is its fluctuation compared to the average value  $U_i$  (with  $U_i = \bar{u}_i$  and  $\bar{u}'_i = 0$ ).

The average of this decomposition therefore makes it possible to remove the fluctuating variables. The average was applied to the continuity and Navier-Stokes equations for incompressible flow by decomposing the variables  $u$  and  $P$ . These equations are given in Eqn. 2 and Eqn. 3.

$$\frac{\partial U_i}{\partial x_i} = 0 \tag{2}$$

$$\frac{\partial U_i}{\partial t} + U_j \frac{\partial U_i}{\partial x_j} = -\frac{1}{\rho} \frac{\partial P}{\partial x_i} + \nu \frac{\partial^2 U_i}{\partial x_i \partial x_j} - \frac{\partial \overline{u'_i u'_j}}{\partial x_j} \tag{3}$$

Where  $\rho$  the specific density,  $P$  the average value of the pressure and  $\nu$  the kinematic viscosity of the fluid. An additional term appeared, namely in Eqn. 4:

$$-\frac{\partial \overline{u'_i u'_j}}{\partial x_j} \tag{4}$$

One approach for closing these equations is to use the Boussinesq approximation defined in Eqn. 5:

$$-\rho \overline{u'_i u'_j} = \mu_t \left( \frac{\partial u_i}{\partial x_j} + \frac{\partial u_j}{\partial x_i} \right) - \frac{2}{3} \left( \rho k + \mu_t \frac{\partial u_k}{\partial x_k} \right) \delta_{ij} \tag{5}$$

Where,  $\mu_t$  is the turbulent viscosity,  $k$  is the turbulent kinetic energy and  $\delta_{ij}$  is the Kronecker symbol. The turbulent viscosity  $\mu_t$  can be obtained by solving additional transport equations. The number of these equations depends on the chosen turbulence model. In this work, the emphasis will be on the k- $\omega$  (SST) model [31].

*3.1.2. Turbulence model k- $\omega$  (SST)*

The k- $\omega$  SST (Shear Stress Transport) model developed by (Menter, 1994) combines the precision of the k- $\omega$  model in the near wall and the k- $\epsilon$  model in the far field region. Such an approach was made by transforming the model k- $\epsilon$  into a k- $\omega$  formulation with the addition of a blending function between the two regions [32]. The k- $\omega$  (SST) model is capable of modeling a wide range of flow profiles with increased precision. The transport equations for the k- $\omega$  (SST) model are given by the Eqn. 6 and the Eqn.7.

$$\frac{\partial}{\partial t} (\rho k) + \frac{\partial}{\partial x_i} (\rho k u_i) = \frac{\partial}{\partial x_j} \left[ \Gamma_k \frac{\partial k}{\partial x_j} \right] + \tilde{G}_k - Y_k \tag{6}$$

$$\frac{\partial}{\partial t} (\rho \omega) + \frac{\partial}{\partial x_i} (\rho \omega u_i) = \frac{\partial}{\partial x_j} \left[ \Gamma_\omega \frac{\partial \omega}{\partial x_j} \right] + G_\omega - Y_\omega + D_\omega \tag{7}$$

$\tilde{G}_k$  and  $G_\omega$  represent the production conditions of  $k$  and  $\omega$ .  $Y_k$  and  $Y_\omega$  represent the terms of dissipation of  $k$  and  $\omega$ .  $\Gamma_k$  and  $\Gamma_\omega$  represent the effective diffusivity of  $k$  and  $\omega$ . Finally,  $D_\omega$  represents the term of cross diffusion. The turbulent kinetic energy  $k$  and specific dissipation rate  $\omega$  are determined as in the Eqn. 8 and the Eqn.9. These equations are used to calculate the initial conditions parameters.

$$k = \frac{3}{2} (U_0 I)^2 \tag{8}$$

$$\omega = \rho \frac{k}{\mu} \left( \frac{\mu_t}{\mu} \right)^{-1} \tag{9}$$

Where  $U_0$  is the mean velocity and  $I$  the turbulence intensity defined as the ratio of the root-mean-square of the velocity fluctuations  $u'_i$  to the mean flow velocity  $U_i$ . A blending function  $F_1$ , between the near wall region and the far field was integrated in the terms of the production derivation, dissipation, diffusivity and cross diffusion as in Eqn 10.

$$\phi = F_1\phi_1 + (1 - F_1)\phi_2 \quad (10)$$

Where  $\phi_1$  regroup all the constants of the original  $k-\omega$  model and  $\phi_2$  regroup all the constants of the transformed  $k-\epsilon$  model.  $\phi$  is the resulting constant of the model and  $F_1$  is the blending function, which is equal to one in the near wall and zero far from the surface.

### 3.2. Aerodynamics coefficients

Determining the air stresses on the car consists in measuring the main component of the aerodynamic torsor, which is the drag coefficient. It is the ratio of the aerodynamic torsor, to the dynamic pressure relative to the reference velocity, over the projected area in the main direction of flow. It is defined as:

$$C_D = \frac{F_x}{\frac{1}{2}\rho U_0^2 S_x} \quad (11)$$

## 4. Numerical study

### 4.1. Geometry and mesh of the 3D model

A 3D model was created and simulated on the ANSYS software. Since steady flow was assumed, a XOZ symmetry plane was used to cut the model in half to reduce the computational time. The dimensions of the simulation area are  $11044 \times 1194.5 \times 1839$  mm. The upstream and downstream boundary distances from the body were respectively 3.26 L and 6.32 L. The upper wall of the far field is 1.5 L and the width of the domain is 1 L (where L is the length of the model). These dimensions are recommended by ERCOFTAC in the modeling of refined turbulence [33]. The dimensions of the computation domain imply a blocking factor equal to 5.23%. To capture the flow on the boundary layer, a coefficient of  $y^+ = 1$  was chosen. The rate of expansion of the mesh starting from the boundary layer of the model is 1.2. The mesh elements are hexahedral near the model contours and the bottom wall of the domain, and tetrahedral in the far field region (Figure 3). The boundary conditions are presented in Table 2. Numerical calculations were carried out on a CPU of 3 processors and 8 GB of RAM. The residuals of the equations of continuity, velocity and  $k-\omega$  are limited to  $10^{-6}$ . The second-order upwind scheme was employed for the terms of the momentum and turbulence closure model equations [34].

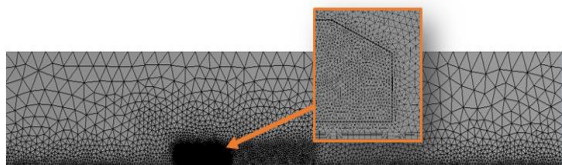


Figure 3. Mesh of the domain around Ahmed's model

Table 2. Boundary conditions

Zone	Boundary conditions	Inputs parameters
Upstream	Velocity-Inlet	$u_x = U_0$ ; $u_y = 0$ ; $u_z = 0$
Downstream	Pressure-Outlet	free
Road	Wall	$u_x$ ; $u_y$ ; $u_z = 0$
Top	Wall	$u_x$ ; $u_y$ ; $u_z = 0$
Symmetry	Symmetry	$u_x = U_0$ ; $u_y = 0$
Side	Wall	$u_x$ ; $u_y$ ; $u_z = 0$
Ahmed model	Wall	$u_x$ ; $u_y$ ; $u_z = 0$

### 4.1. Study of the mesh sensitivity

To ensure an independent solution of the mesh for all the simulations, a sensitivity study was carried out on the model of Ahmed without deflector, for the Reynolds number of  $7.89 \times 10^5$ . Three types of meshes M1, M2 and M3 were used and are coarse, medium and fine mesh, respectively. The percentage difference in the drag coefficient ( $C_D$ ) between two successive meshes was less than 3% (Table 3). For M2 (664 818 elements), increasing the number of elements by 53.1% to obtain M3 (1 417 521 elements), gives 2.88 % change in ( $C_D$ ). Globally, a mesh independence solution was obtained for M2. Therefore, this mesh will be used for all other simulations.

Table 3. Mesh sensitivity

Mesh	No. elements	Drag coefficient ( $C_D$ )	Difference
M1	287 819	0.3001	6.07 %
M2	664 818	0.2819	2.88 %
M3	1 417 521	0.2738	--

### 4.2. Comparison with literature

For a Reynolds number  $Re = 7.89 \times 10^5$  corresponding to the inlet velocity  $U_0 = 40 \text{ m.s}^{-1}$ , the value of the mean mesh (M2) is compared with the data in the literature (Table 4). The differences of the drag coefficient obtained compared to (Thomas and Agarwal)  $k-\omega$  SST [35] and (Guilmineau et al.) EARSM [36] are respectively 2.46 % and 0.53 %. These values may be due to the refinement of the mesh and the difference in the number of elements used. For the experimental data, a difference of 1.09 % was observed compared to (Ahmed et al.) [28] and of 5.92 % compared to (Meile et al.) [37].

Table 4. Comparison of the drag coefficient obtained with the literature

Type of study	Drag coefficient ( $C_D$ )
Present work	0.2819
(Thomas et Agarwal) $k-\omega$ SST [35]	0.2890
(Guilmineau et al.) EARSM [36]	0.2804
(Ahmed et al.) [28]	0.2850
(Meile et al.) [37]	0.2990

## 5. Optimal simulation plan

### 5.1. Plackett-Burman Plan Concept

Plackett-Burman plan is generally 2-level, resolution III screening designs. In this category of design, the main

effects are aliased with the two-factor interactions. The design of the Plackett-Burman plan is an efficient screening method for identifying the important factors among a large number of factors that influence a Y response [38].

5.2. Definition of factors

Eight factors were raised on the deflector installed on the rear window of Ahmed's body, namely: i) Length ratio (A); ii) Width ratio (B); iii) Thickness (C); iv) Ends angle (D); v) Angle of inclination (E); vi) Type of curvature (F); vii) Radius of curvature (G) and viii) Inlet velocity (H). Each factor was evaluated based on two levels: (-1) for the low level and (+1) for the high level (Table 5).

The choice of these factors, as well as their levels, is obtained mainly from the preliminary study carried out as well as the bibliographic data of previous works [8,24,29,30]. The application of the Plackett-Burman model in current research has identified a series of 12 parameter combinations to be analyzed on the ANSYS simulation software to optimize the deflector. JMP Pro 14 software was used for the experimental design and data analysis of the model. Figure 4 summarizes the 12 tests of the Plackett-Burman plan selected. The 3D drawings of the Ahmed model with deflector, of the different configurations are made by the CAD software SolidWorks.

Table 5. Levels of factors tested by the Plackett-Burman plan

ID	Factors	Symbol	Numerical Value	
			Low Level (-)	High Level(+)
A	Length Ratio	$l_D/L$ [%]	3	6
B	Width Ratio	$w_D/W$ [%]	50	100
C	Thickness	$Th$ [m]	0.001	0.005
D	Ends angle	$\alpha$ [°]	0	45
E	Angle of inclination	$\theta$ [°]	-5	5
F	Type of curvature	CO	Concave	Convex
G	Radius of Curvature	R [m]	0.05	0.5
H	Inlet velocity	$U_0$ [m.s <sup>-1</sup> ]	20	40

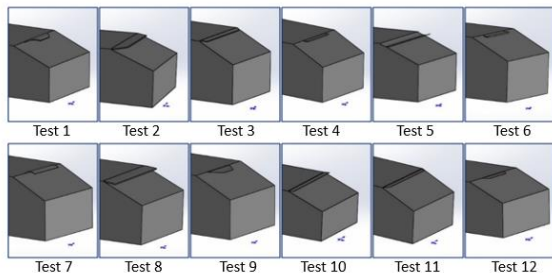


Figure 4. Deflector installed on the rear slant of the Ahmed model according to the 12 tests provided by the Plackett-Burman plan.

6. Results and Discussion

Statistical analysis of the obtained results was performed to evaluate the analysis of the variance between factors (ANOVA). The analysis includes the

Fisher Snedecor test (F test), its associated probability P(F), and the coefficient of determination ( $R^2$ ), which measures the fit quality of the regression model. The experimental design as well as data analysis of the model were carried out via the JMP Pro 14 software.

6.1. Matrix of Experiences

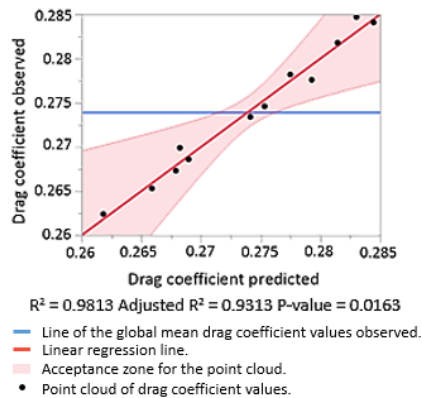
Table 6 presents the model matrix of the simulation and forecast results after a numerical study on the ANSYS simulation software of the various tests given by the Plackett-Burman plan. From the results obtained, it can be seen that the best simulation conditions leading to a remarkable drag coefficient ( $C_D = 0.2624$ ) were observed during the following combination: length ratio (6 %); width ratio (50 %); thickness (0.001 m); ends angle (0 °); angle of inclination (5 °); type of curvature (Concave); radius curvature (0.05 m) and inlet velocity (40 m.s<sup>-1</sup>). This configuration is associated to a predicted value of response at the level of the aerodynamic drag ( $C_D = 0.2618$ ).

Table 6. Matrix of test results established by the Plackett-Burman plan

TEST	Drag Coefficient	
	Simulation result	Predicted result
1	0.2673	0.2679
2	0.2746	0.2753
3	0.2699	0.2682
4	0.2847	0.2830
5	0.2818	0.2814
6	0.2776	0.2793
7	0.2624	0.2618
8	0.2686	0.2690
9	0.2782	0.2775
10	0.2653	0.2659
11	0.2841	0.2845
12	0.2734	0.2741

6.2. Quality assessment of the numerical model

Figure 5 shows a linear regression analysis of the observed drag coefficient values obtained by numerical simulation using ANSYS Fluent, versus predicted values of the JMP Pro 14. There is a regular and close distribution of the numerical values on either side of the theoretical line. It is observed that the value of  $R^2 = 0.9813$  and adjusted  $R^2 = 0.9313$  are significantly very close, this justifies that the value of the observed variation is explained by the direct effects of factors. Furthermore, the value of  $R^2$ , which is very close to one, shows that the chosen Plackett-Burman plan has a high quality in the level of fitting.



**Figure 5.** Graphical representation of the observed values versus the predicted response ones (Y).

### 6.3. Analysis of variance (ANOVA)

The appropriateness of the chosen model has been assessed by ANOVA analysis. This test was used to analyze the variance of the model established with respect to the variance of the residue, using the Fisher Snedecor test. The result was taken to be significant if ( $F_{exp} \gg F_{\alpha, v \text{ model}, v \text{ residue}}$ ), where  $v \text{ model} = 8$ ,  $v \text{ residue} = 3$  and  $\alpha = 0.05$ . The results of the analysis of variance carried out show that the experimental value  $F_{exp} = 19.6850$ , which is the ratio between the mean square of the model and the mean square of the error, is much higher than the critical value  $F_{(theo.)} = F_{(0.05 (8) (3))} = 8.85$  of the distribution  $F$  at a confidence interval of 5% at 8 and 3 degrees of freedom. In addition, the probability  $\text{Prob.} > F_p = 0.0163$  was significantly inferior to 0.05. Consequently, the model for the coefficient of drag is validated.

### 6.4. Equation of the model according to the most influential factors

From the statistical analysis, it was observed that the aerodynamic drag of the model was significantly influenced by the type of curvature (F), the inlet velocity (H) and the length ratio (A). However, the impact of the other parameters were not significant, because, their p-value were higher than 0.05. The best model, which gives the determining factors that have a significant influence in the calculation of the drag coefficient of the Ahmed body with deflector installed on the rear window, is written as the Eqn. 12.

$$Y = 0.2740 - 0.0062F - 0.0027H - 0.0018A \quad (12)$$

### 6.5. Optimal deflector

A model of Ahmed with a deflector was designed on SolidWorks by using the optimal factors obtained from JMP Pro 14 software (Figure 6). The numerical study was conducted on the ANSYS Fluent software. After about 550

iterations, the convergence of the residuals of the simulation was observed. Table 7 presents a comparison between the value of the drag coefficient obtained by the JMP Pro 14 software, according to the Plackett-Burman screening plan ( $C_D = 0.261951$ ), and the value obtained by the numerical study on the CFD Fluent software ( $C_D = 0.265789$ ). It is observed that the value obtained by the screening plan is slightly inferior to that obtained by the numerical simulation, with a relative deviation estimated at 1.465%. The value obtained by the simulation allows a drag reduction of up to 5.75% compared to the Ahmed's body without deflector.

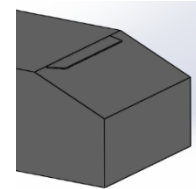


**Figure 6.** Deflector installed on the Ahmed model according to the optimal factors obtained by JMP Pro 14.

**Table 7.** Optimal values of the factors and the obtained drag coefficient

ID	Optimal Values	Drag Coefficient obtained		Relative Gap [%]
		Plackett-Burman Plan	Simulation	
A	6%			
B	100%			
C	0.003 m			
D	0°	0.261951	0.265789	1.465
E	4.5°			
F	Concave			
G	0.275m			
H	40 m.s <sup>-1</sup>			

Figure 7 below represents a comparison of the turbulent kinetic energy (TKE) in the plane of symmetry of Ahmed's model for two cases (without and with a deflector obtained from the optimal factors). The maximum TKE values were observed to be in the closest wake zone to the base of the model. For the first case (Model without deflector), there is a high concentration of TKE in the wake zone of the model near the ground between  $X = 0.1$  m and  $X = 0.2$  m. In this case, the size of the main vortices has been increased. On the contrary, in the second case (Ahmed's model with deflector obtained from the optimal factors), the wake zone is lengthened and the vortices dissipated. The maximum TKE was weakened and moved away from the model to be at position  $X = 0.25$  m. It is found that the use of this type of deflector delays separation and disturbs vortices, which minimizes the depression created in the wake zone behind the vehicle, and then it decreases its aerodynamic drag.

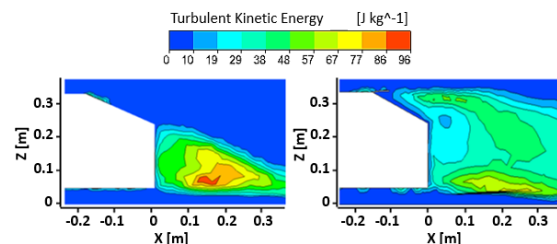


**Figure 7.** Comparison of the turbulent kinetic energy for the Ahmed model without deflector (left), and the model with optimal deflector (right).

## 7. Conclusion

The evaluation of the effect of many factors related to the deflector installed on the rear base of the Ahmed model was carried out via the screening concept. To determine the deflector factors that influence aerodynamic drag of cars, the Plackett-Burman plan was first used. Eight factors were analyzed and identified on two levels, namely: length ratio (3 % - 6 %), width ratio (50 % - 100 %), thickness (0.001 m - 0.003 m), ends angle (0 ° - 45 °), angle of inclination (-5 ° - 5 °), type of deflector (Convex, Concave), radius of curvature (0.05 m - 0.5 m) and inlet velocity (20 m.s<sup>-1</sup> - 40 m.s<sup>-1</sup>). Twelve study models were performed by the SolidWorks software.

Besides, the numerical simulation was performed on the CFD software ANSYS. The impact of these factors was studied on a response (Y) which represents the coefficient of aerodynamic drag. The JMP Pro 14 software gives three significant factors: the type of deflector, the inlet velocity and the length ratio. The drag coefficient obtained from the optimal values was compared to that of simulation and thus a relative deviation of 1.46 % was observed. There was a reduction of about 5.75 % in the drag observed on Ahmed's model with optimal deflector, compared to the non-deflector model. In addition, installing the optimal deflector on the body of Ahmed widens the wake area and eliminates chain stay vortex.

## Author Contributions

Conceptualization, M.M. and M.O.; methodology, B.N.; software, M.M.; validation, M.O., O.B.; formal analysis, M.M.; investigation, M.M.; resources, B.N.; data curation, M.M.; writing—original draft preparation, M.M.; writing, review and editing, M.M.; visualization, M.O.; supervision, O.B.; project administration, M.O. All authors have read and agreed to the published version of the manuscript.

## Funding

This research received no external funding.

## Declaration of Competing Interest

The authors declare that they have no known competing financial interests or personal relationships that could have appeared to influence the work reported in this paper.

## References

- [1] F. Szodrai, "Quantitative Analysis of Drag Reduction Methods for Blunt Shaped Automobiles", *Applied Sciences*, vol. 10, n° 12, 2020, p. 4313.
- [2] M. Maine, M. E. Oumami, O. Bouksour, A. Tizliouine, "Review of research on cars wake flow control methods to reduce aerodynamic drag", *International journal of innovation and applied studies*, 2019, 25:1069-1089.
- [3] B. Wang, Z. Yang, H. Zhu, "Active flow control on the 25° Ahmed body using a new unsteady jet", *International Journal of Heat and Fluid Flow*, vol. 79, 2019, p. 108459.
- [4] T. Heinemann, M. Springer, H. Lienhart, S. Kniesburges, C. Othmer, S. Becker, "Active flow control on a 1:4 car model", *Experiments in Fluids*, vol. 55, n° 5, 2014.
- [5] A. A. Moussa, R. Yadav, J. Fischer, "Aerodynamic Drag Reduction for A Generic Sport Utility Vehicle Using Rear Suction", vol. 4, n° 8, 2014, p. 7.
- [6] M. Metka, J. W. Gregory, "Drag reduction on the 25-deg Ahmed model using fluidic oscillators", *Journal of Fluids Engineering*, vol. 137, n° 5, 2015, p. 051108.
- [7] Shimizu K, Nakashima T, Sekimoto S, Fujii K, Hiraoka T, Nakamura Y, Nouzawa T, Ikeda J, Tsubokura M., "Aerodynamic drag reduction of a simplified vehicle model by promoting flow separation using plasma actuator", *Mech. Eng. Lett.*, (5):1-9, 2019.
- [8] A. Hossain, P. R. Arora, A. Rahman, A. A. Jaafar, "Analysis of Longitudinal Aerodynamic Characteristics of an Aircraft Model with and Without Winglet", *Jordan Journal of Mechanical and Industrial Engineering*, vol. 2, n° 3, 2008, p. 143-150.
- [9] A. Hossain, A. Rahman, J. Hossen, P. Iqbal, N. Shaari, et G. K. Sivaraj, "Drag reduction in a wing model using a bird feather like winglet", *Jordan Journal of Mechanical and Industrial Engineering*, vol. 5, n° 3, 2011, p. 267-272.
- [10] G. Fourrié, L. Keirsbulck, L. Labraga, P. Gilliéron, "Bluff-body drag reduction using a deflector", *Experiments in Fluids*, vol. 50, n° 2, 2011, p. 385-395.
- [11] R. B. Sharma, R. Bansal, "CFD simulation for flow over passenger car using tail plates for aerodynamic drag reduction", *IOSR Journal of Mechanical and Civil Engineering (IOSR-JMCE)*, vol. 7, n° 5, 2013, p. 28-35.
- [12] E. Wahba, H. Al-Marzooqi, M. Shaath, M. Shahin, T. El-Dhmarshawy, "Aerodynamic drag reduction for ground vehicles using lateral guide vanes", *CFD Letters*, vol. 4, n° 2, 2012, p. 68-79.
- [13] S. Bayraktar, Y. O. Bilgili, "Effects of under body diffuser on the aerodynamics of a generic car", *International Journal of Automotive Engineering and Technologies*, vol. 7, n° 2, 2018, p. 99-109.
- [14] A. Dubey, S. Chheniya, A. Jadhav, "Effect of Vortex generators on Aerodynamics of a Car: CFD Analysis", *Inter. Journal of Innovations in Engineering and Technology*, vol. 2, n° 1, 2013, p.137-144.
- [15] G. Pujals, S. Depardon, C. Cossu, "Drag reduction of a 3D bluff body using coherent streamwise streaks", *Experiments in fluids*, vol. 49, n° 5, 2010, p. 1085-1094.
- [16] Y. Wang, C. Wu, G. Tan, Y. Deng, "Reduction in the aerodynamic drag around a generic vehicle by using a non-smooth surface", *Proceedings of the Institution of Mechanical Engineers, Part D: Journal of Automobile Engineering*, vol. 231, n° 1, 2017, p. 130-144.
- [17] T. Hirst, C. Li, Y. Yang, E. Brands, G. Zha, "Bluff body drag reduction using passive flow control of Jet Boat Tail", *SAE International Journal of Commercial Vehicles*, vol. 8, n° 2, 2015, p. 713-721.
- [18] B. Mohammadikalakoo, P. Schito, M. Mani, "Passive flow control on Ahmed body by rear linking tunnels", *Journal of Wind Engineering and Industrial Aerodynamics*, vol. 205, 2020, p. 104330.
- [19] F. Delassaux, I. Mortazavi, E. Itam, V. Herbert, C. Ribes, "Sensitivity analysis of hybrid methods for the flow around the Ahmed body with application to passive control with rounded edges", *Computers & Fluids*, vol. 214, 2021, p. 104757.
- [20] B. Khalighi, K.-H. Chen, G. Iaccarino, "Unsteady aerodynamic flow investigation around a simplified square-back road vehicle with drag reduction devices", *Journal of fluids engineering*, vol. 134, n° 6, 2012, p. 061101.
- [21] M. Varney, M. Passmore, A. Gaylard, "The Effect of Passive Base Ventilation on the Aerodynamic Drag of a Generic SUV Vehicle", *SAE Int. J. Passeng. Cars - Mech. Syst.*, vol. 10, n° 1, 2017, p. 345-357.
- [22] R. Tarakka, N. Salam, J. Jalaluddin, M. Ihsan, "Effect of blowing flow control and front geometry towards the reduction of aerodynamic drag on vehicle models", *FME Transactions*, vol. 47, n° 3, 2019, p. 552-559.
- [23] A. R. Paul, A. Jain, F. Alam, "Drag reduction of a passenger car using flow control techniques", *International Journal of Automotive Technology*, vol. 20, n° 2, 2019, p. 397-410.

- [24] W. Hanfeng, Z. Yu, Z. Chao, H. Xuhui, "Aerodynamic drag reduction of an Ahmed body based on deflectors", *Journal of Wind Engineering and Industrial Aerodynamics*, vol. 148, 2016, p. 34-44.
- [25] S. Krajnović, "Optimization of aerodynamic properties of high-speed trains with CFD and response surface models", in *The Aerodynamics of Heavy Vehicles II: Trucks, Buses, and Trains*, vol. 41, 2009, p. 197-211.
- [26] W. Zheng, W. Hu, J. Hai-jun, S. Ya-feng, "Study on Response Surface Methodology with Artificial Neural Networks Application in Aerodynamic Optimization", in *2009 WRI World Congress on Computer Science and Information Engineering*, Los Angeles, California USA, 2009, p. 620-626. doi: 10.1109/CSIE.2009.458.
- [27] S. Beigmoradi, H. Hajabdollahi, A. Ramezani, "Multi-objective aero acoustic optimization of rear end in a simplified car model by using hybrid Robust Parameter Design, Artificial Neural Networks and Genetic Algorithm methods", *Computers & Fluids*, vol. 90, 2014, p. 123-132.
- [28] S. R. Ahmed, G. Ramm, G. Faltin, "Some Salient Features Of The Time-Averaged Ground Vehicle Wake", in *SAE International Congress and Exposition*, 1984.
- [29] A. Raina, G. A. Harmain, M. I. U. Haq, "Numerical investigation of flow around a 3D bluff body using deflector plate", *International Journal of Mechanical Sciences*, vol. 131-132, 2017, p. 701-711.
- [30] A. Raina, A. Khajuria, « Flow control around a 3D-bluff body using passive device, *EPH-International Journal of Science and Engineering (ISSN: 2454-2016)*, vol. 4, n° 1, 2018, p. 08-13.
- [31] A. L. J. Pang, M. Skote, S. Y. Lim, "Modelling high Re flow around a 2D cylindrical bluff body using the  $k-\omega$  (SST) turbulence model", *Progress in Computational Fluid Dynamics*, An International Journal, vol. 16, n° 1, 2016, p. 48-57.
- [32] F. R. Menter, "Two-equation eddy-viscosity turbulence models for engineering applications", *AIAA Journal*, vol. 32, n° 8, 1994, p. 1598-1605.
- [33] R. Manceau, J. P. Bonnet, M. Leschziner, F. Menter, "10th joint ERCOFTAC (SIG-15)/IAHR/QNET-CFD workshop on refined flow modelling", *Universite de Poitiers*, 2002.
- [34] C. A. R. Duarte, L. E. R. Duarte, B. S. de Lima, F. J. de Souza, "Performance of an optimized  $k-\epsilon$  turbulence model for flows around bluff bodies", *Mechanics Research Com.*, vol. 105, 2020, p. 103518.
- [35] B. Thomas, R. K. Agarwal, "Evaluation of various RANS turbulence models for predicting the drag on an Ahmed body", in *AIAA Aviation 2019 Forum*, Dallas, Texas, juin 2019.
- [36] E. Guilmineau, G. B. Deng, A. Leroyer, P. Queutey, M. Visonneau, J. Wackers, "Assessment of hybrid RANS-LES formulations for flow simulation around the Ahmed body", *Computers & Fluids*, vol. 176, 2018, p. 302-319.
- [37] W. Meile, G. Brenn, A. Reppenhagen, B. Lechner, A. Fuchs, "Experiments and numerical simulations on the aerodynamics of the Ahmed body", vol. 3, p. 32-39, 2011.
- [38] R. L. Plackett, J. P. Burman, "The design of optimum multifactorial experiments", *Biometrika*, vol. 33, n° 4, 1946, p. 305-325.